Investigation of resonance structures in optically thin solar cells

Maren Anna Brandsrud,[a,*] **Reinhold Blümel**,[b] **Rozalia Lukacs**,[a] **Eivind Seim**,[a] **Erik Stensrud Marstein**,[c,d] **Espen Olsen**,[a] **and Achim Kohler**[a]

[a]Norwegian University of Life Sciences, Faculty of Science and Technology, Drøbakveien, Norway

[b]Wesleyan University, Department of Physics, Middletown, Connecticut, United States

[c]Institute for Energy Technology, Department of Solar Energy, Kjeller, Norway

[d]University of Oslo, Department of Technology Systems, Kjeller, Norway

Abstract. To reduce costs, the solar cell industry aims at producing thinner solar cells. Structuring the surfaces of optically thin devices is important for avoiding transmission-related losses and, hence, increasing their efficiency. Light trapping leads to longer optical pathlengths and increased absorption of energy. In addition, resonances in the nanostructures enhance the absorption in the energy-converting material. Further, resonances in periodic structures may couple with each other and thereby increase the absorption. Here, we establish a model system consisting of a multilayered solar cell to study resonances and coupling of resonances in a one-dimensional system. We show that resonances in energy-converting and nonenergy converting layers exist, evaluate the resonances and the coupling of resonances in different thin-film systems, and show how they affect the total absorption of energy in the energy-converting layer. We optimize the parameters of the multilayered thin-film systems to achieve an increase in the amount of the absorbed energy. We find that resonances in nonabsorbing material at the top may lead to absorption enhancement, while we cannot find any enhancement effect due to the coupling of resonances. [DOI: 10.1117/1.JPE.11.024501]

Keywords: optically thin solar cells; resonance enhancement; conversion efficiency; coupling of resonances.

Paper 21003 received Jan. 12, 2021; accepted for publication Jun. 4, 2021; published online Jun. 22, 2021.

1 Introduction

The solar-cell industry is continuously looking for ways to reduce material usage in the production of solar cells while maintaining conversion efficiency to increase the cost efficiency of solar-cell devices.[1,2] Although thin, silicon solar cells exhibit lower absorption than thicker, traditionally crystalline silicon wafer cells,[1] absorption in optically thin solar cells can be enhanced by surface structuring, e.g., by adding surface structures to the top layer of thin solar cells.[3,4] The most established approach is light trapping, wherein the pathlength of light in the absorber is increased because of the surface structures. Light trapping is common in surface-structure solar cells in which the surface structures are larger than the wavelength employed, i.e., in the short wavelength limit. It has also been shown that nanostructured surfaces cause resonances in the electric field that increases the absorption of light in the absorptive material below.[3] Coupling of resonances into the nanostructures has also been discussed as a mechanism for absorption enhancement in structured thin-film solar cells.[5,6] A different mechanism that has been used to address enhancement of absorption efficiency of thin solar cells is the minimization of the energy losses due to reflection.[7] A possible way to achieve this is to add one or more thin dielectric layers on the top of the solar cell as an antireflection coating (ARC). While single layer

*Address all correspondence to Maren Anna Brandsrud, maren.brandsrud@nmbu.no

ARCs are standard in the industry today, many studies have been carried out to optimize thin-film solar cells consisting of two different layers to find an optimal combination of the refractive indices and thicknesses of the materials.[8]

The aim of this paper is to study the absorption efficiency in the energy converting layer of a solar cell as a function of the appearance of resonances in the absorbing and nonabsorbing layers of a thin-film solar cell. For this purpose, we developed a simple model system that exhibits resonances and allows us to investigate the implication of these resonances on absorption in the energy-converting material. A simple system that can exhibit resonances is a multilayered film system. A multilayered film system can be set up by absorbing and nonabsorbing layers. It can be used to investigate how resonances in the nonabsorbing layers affect the absorption in the absorbing layers. It can be further used to investigate how absorption can be enhanced by tuning the refractive index and the thicknesses of the absorbing and nonabsorbing layers involved. Therefore, our work is strongly related to the optimization of ARCs,[7] but it focuses on a different aspect, namely the effect of resonances in layered films on the absorption in the energy-converting film.

To study the effectiveness of the device, we evaluate the absorption efficiency, σ_a.[9–11] To take into account the characteristics of the solar spectrum, absorption efficiency can be multiplied by the solar spectrum. The resulting quantity is called the optical generation rate.[12] The systems evaluated in this study are three-dimensional (3D) systems in which the incoming light is a plane wave propagating toward the system and the propagation direction is perpendicular to the surfaces. Because of normal incidence, the systems are invariant in two dimensions and are effectively one-dimensional (1D) systems. The results presented for normal incidence to a film are directly transferable to the same system with oblique incidence. Oblique incidence results in a reduced normal component of the wave vector. Therefore, oblique incidence leads to a simple shift of the resonance structure with respect to the wavelength region, and the same reasoning can be applied for normal incidence.[13]

By including the wavelength-dependent refractive index, we show that the results can be used to optimize solar cell designs with respect to absorption.

The paper is organized as follows. In Sec. 2, we present the systems that we evaluate and relevant theory. In the first part of Sec. 3 (Secs. 3.1–3.3), we evaluate the systems with wavelength-independent refractive indices. We investigate how the absorption efficiency and the resonance structure in the layered films depend on the size of the imaginary part of the refractive index. We show that our results agree with the Fresnel equations[14] for nonmagnetic dielectric materials. We investigate further if the thickness of the layers can be optimized with respect to absorption efficiency and material usage. We show how resonances in the nonabsorptive material enhance the absorption of light in the energy-converting film. In Section 3.3, we evaluate how two nonabsorptive layers can be used to increase the absorption efficiency. We evaluate the effect of coupling of resonances between nonabsorptive layers, when the absorptive layer is between two nonabsorptive films. We evaluate how the coupled resonances of the two nonabsorptive layers and resonances in the absorptive layer can affect the absorption efficiency. In Sec. 3.4, we further demonstrate that our approach can be useful in the optimization of real solar-cell material by optimizing the thickness of the layers of an experimentally realizable solar cell. In Sec. 4, we discuss our results; we summarize and conclude our paper in Sec. 5.

2 Theory

Optically thin solar cells consisting of layers, with normal incidence light, can be treated as 1D systems and are therefore simple to handle numerically. The model system chosen in this paper represents a 1D system consisting of several thin layers with different absorbing and nonabsorbing materials. Both the nonabsorbing and the absorbing materials can function as resonators, as shown later in the paper. The systems that are investigated are shown in Fig. 1. For all systems, a plane wave with an amplitude equal to one is propagating toward the layers from the left. Figure 1(a) shows the simplest system, consisting only of a boundary between air and the absorptive material of refractive index n_a. The absorption properties of the absorptive film are described by the imaginary part of n_a. In Fig. 1(a), the thickness of the absorptive material is assumed to be infinite. In the system presented in Fig. 1(b), a single absorptive film of thickness a_a and

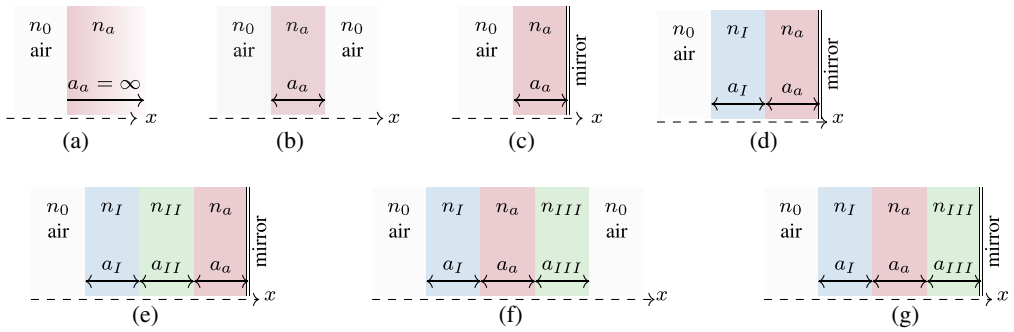

Fig. 1 The systems evaluated are 1D systems. The incident light is a plane wave of amplitude equal to 1 propagating from the left with the refractive index of $n_0 = 1$. In system (a), the system consists of a boundary between n_0 and the absorptive material with a refractive index of n_a and an infinite thickness. The system in (b) consists of a finite absorptive film with refractive index n_a and a thickness a_a. System (c) is identical to system (b) except that a perfect mirror is placed behind the film. Systems (d) and (e) have the absorptive film placed behind one or two nonabsorptive layers. A mirror is placed behind the absorptive film. The thicknesses of the nonabsorptive films are a_I and a_{II}, and the refractive indices are n_I and n_{II}. System (f) has the absorptive layer between the nonabsorptive layers with thicknesses a_I and a_{III} and refractive indices n_I and n_{III}. System (g) is equivalent to system (f) but has a back side mirror behind the third layer.

refractive index n_a is shown. For Figs. 1(c)–1(e), we assume a back side mirror behind the layers, reflecting back all radiation perfectly. The thickness of the absorptive layer is a_a and has a refractive index of n_a. The refractive indices of the nonabsorptive layers are n_I and n_{II} with thicknesses of a_I and a_{II}. The system presented in Fig. 1(f) is the system used to evaluate a coupling between the nonabsorptive layers on each side of the absorptive layer. Figure 1(g) shows an identical system to the one shown in Fig. 1(f), but with a back side mirror behind the third layer.

Since we only consider normal incidence and thus treat the model system in 1D, we do not need to consider the polarization. The model system can, therefore, be described by the scalar wave theory, which provides an exact description of the wave mechanics in the film structures. The 1D model is completely equivalent to the 3D film system with normal incident light. The wave functions for the systems shown in Fig. 1 are shown in Table 1. The amplitudes of the wave functions are found by requiring that the wave functions and their first derivatives are continuous across the boundary.[15]

For layered systems, the amount of absorbed light is calculated via the absorption efficiency σ_a, given as

$$\sigma_a = 1 - |r|^2 - |t|^2, \tag{1}$$

where r is the amplitude of the reflected plane wave and t is the amplitude of the transmitted wave.[9,10,16] The reflection probability of the system is given by $|r|^2 = R$, and the transmission probability is given by $T = |t|^2$. When the refractive index is real for all films involved, $|r|^2 + |t|^2 = 1$ and the absorption efficiency $\sigma_a = 0$. If a mirror is placed behind the system, there is no transmitted wave, i.e., $t = 0$, and the absorption efficiency is given as

$$\sigma_a = 1 - |r|^2. \tag{2}$$

The amplitude of the reflected wave is found by requiring a continuous scalar wave function and a continuous first derivative of the scalar wave function at all interfaces.[15,16] For simple systems with a few layers of materials, the calculation of σ_a is straightforward. For systems consisting of several layers, the transfer matrix method[17] may be used. Alternatively, a hierarchical summation scheme suggested by Brandsrud et al.[9] is employed.

The absorption efficiency is also related to the absolute value of the scalar wave function, $\psi(x)$, in a 1D system as

$$\sigma_a = 2k \int n_r(x) n_i(x) |\psi(x)|^2 \mathrm{d}x, \tag{3}$$

where k is the angular wave number in vacuum of the incoming wave and the refractive index of the system is given by $n(x) = n_r(x) + in_i(x)$.[9] When the wave function has higher absolute values, we expect that the absorption efficiency increases. Since resonances appear locally and lead therefore locally to increased absorption efficiencies, it is interesting to evaluate if the absorption efficiency increases over the whole solar spectral range for a given system as well. To evaluate if the absorption properties of a layered system are enhanced, the averaged absorption efficiency, $\overline{\sigma}_a$, needs to be considered for whole wave length interval. To take into account the characteristics of the solar spectrum, the integral in Eq. (3) is weighted by the solar spectrum.

The refractive index n is in general wavelength-dependent.[18] In the first part of the paper, we consider thin-film systems with an index of refraction that is independent of the wavelength. In the second part of the paper, we evaluate an experimentally realizable solar cell. The refractive indices of the materials are found experimentally and are wavelength-dependent.

3 Results

In this section, we evaluate the different systems shown in Fig. 1.

3.1 *Single Film*

We start with the system in Fig. 1(a), which consists of an infinitely thick absorptive material with a wavelength-independent refractive index. The system is shown in Fig. 1(a). The real part of the refractive index of the absorptive layer n_a is set to 4.3. This is the real part of the refractive index of silicon at a wavelength equal to 500 nm. We consider a range for the imaginary part of the refractive index, which we vary between 0 and 5. The wavelength interval evaluated is from 250 to 1000 nm. Since the absorptive layer is infinitely deep, all light that enters the absorptive material is absorbed. $\sigma_a(\lambda)$ is shown in Fig. 2(a). For the system containing only one single boundary, the reflection and transmission coefficients r and t do not depend on the wavelength.[9] Figure 2(a) shows that $\sigma_a(\lambda)$ decreases as n_i increases. This is expected since the absolute value of n increases, which results in an increased probability for reflection.[9,16] In Fig. 2(b), the averaged absorption efficiency, $\overline{\sigma}_a$, is shown as a function of n_i. As shown in Fig. 2(a), we observe that an increased n_i is followed by a reduced $\overline{\sigma}_a$

When the absorptive material has a finite thickness that is on the order of the wavelength, standing waves can occur in the film. Figure 2(c) shows $\sigma_a(\lambda)$ for a single absorptive film as shown in Fig. 1(b). The different graphs of $\sigma_a(\lambda)$ correspond to increasing values for n_i. We observe that resonances are present when n_i is sufficiently low. As n_i increases, the resonances are damped, and finally when n_i is large enough, all light is absorbed before it reaches the second boundary and no standing waves can be observed. Figure 2(d) shows how the absorption efficiency averaged over the wavelength range $\overline{\sigma}_a(n_i)$ increases before it reaches a maximum at $n_i = 0.57$.

The system in Fig. 1(c) can be considered a simplified model of a solar cell as it considers one absorptive layer and a mirror on the back side. For such a system, Fig. 2(e) shows the corresponding absorption efficiency $\sigma_a(\lambda)$ for a range of constant imaginary parts of the refractive index. We observe that the resonance structure of $\sigma_a(\lambda)$ changes as we increase the imaginary part of the refractive index. The real part of the refractive index is kept constant, $n_r = 4.3$. As n_i increases we observe the same tendency as for the single film without the mirror. The amplitudes of the resonances are reduced; at one point, all of the light is absorbed before it reaches the mirror, and no standing waves are created. Figure 2(e) shows how the averaged absorption efficiency changes as n_i increases.

Since the absorption efficiency is expected to increase when the absolute value of the wave function increases [see Eq. (3)], it is interesting to consider the wave function for maxima and minima of the absorption efficiency. The system, consisting of a single film with a reflecting back side mirror [Fig. 1(c)], exhibits several maxima for the absorption efficiency in Fig. 2(e),

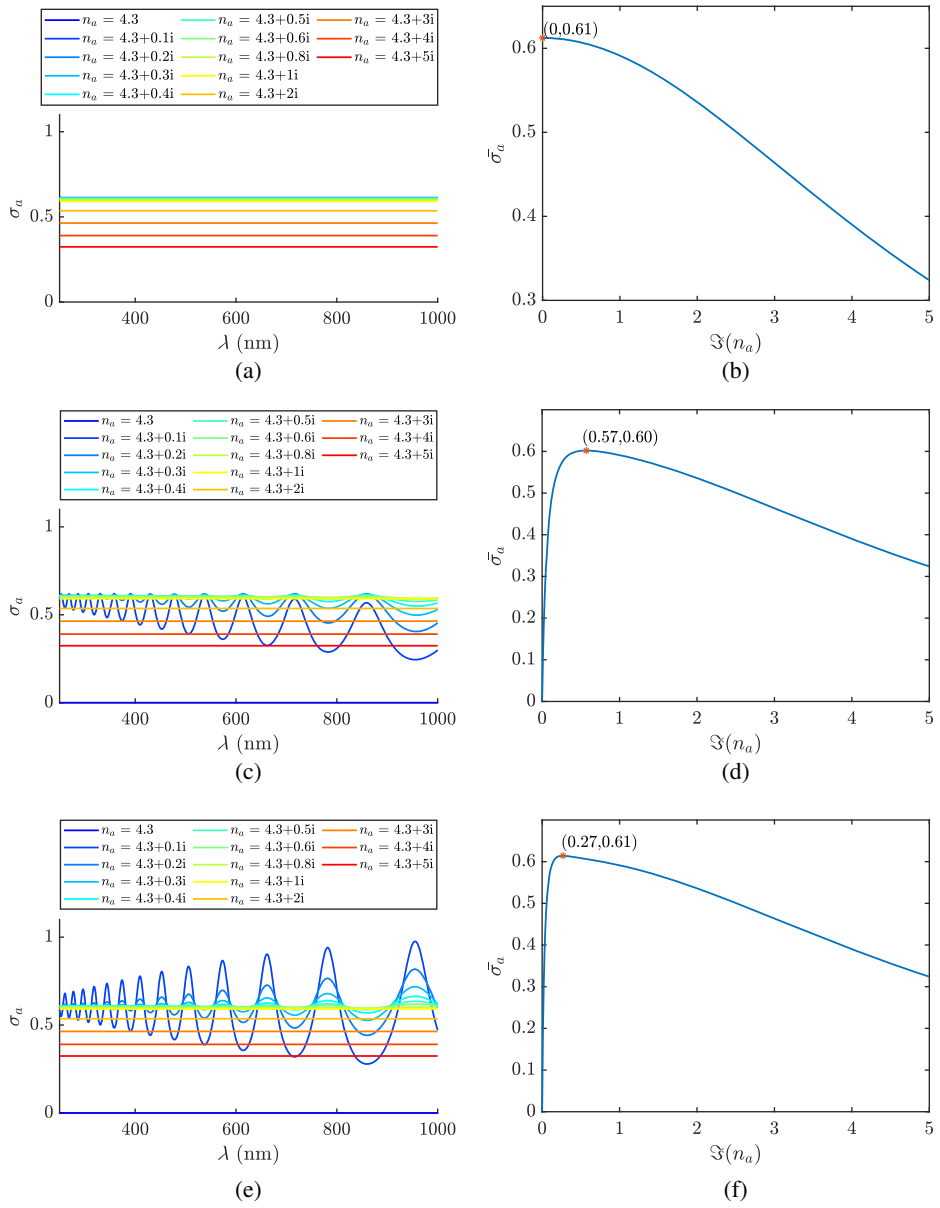

Fig. 2 (a) σ_a as a function of wavelength for an infinitely thick film for increasing $\Im(n_a)$. (b) The averaged absorption efficiency, $\overline{\sigma}_a$, as a function of $\Im(n_a)$ is evaluated. (c) σ_a as a function of wavelength of an absorptive film without a mirror behind. (d) $\overline{\sigma}_a$ as a function of $\Im(n_a)$. (e) and (f) $\sigma_a(\lambda)$ and $\overline{\sigma}_a(\Im(n_a))$ for a system consisting of a single film with a mirror. For all systems, the real part of the refractive index is set to 4.3, which is the real part of the refractive index of silicon at $\lambda = 500$ nm. The investigated wavelength interval is from 250 to 1000 nm. (c)–(f) The thickness of the absorptive film is set to 500 nm.

e.g., for the imaginary part of the refractive index of $0.1i$. We consider the maximum that appears at 662 nm and the minimum that appears at 717 nm. The corresponding wave functions (ψ_c from Table 1) are plotted in Fig. 3 outside and inside the film for two selected wavelengths, 662 nm (red line) and 717 nm (blue line). The refractive index for the film is $4.3 + 0.1i$, and the thickness is 500 nm.

We see that the red line in Fig. 3 corresponds to a peak, a resonance, in $\sigma_a(\lambda)$ [Fig. 2(c)]. We observe that the absolute square of $|\psi|^2$ is larger in the case in which the wavelength corresponds to a maximum in $\sigma_a(\lambda)$.

We now return to the averaged absorption efficiency shown in Fig. 2(f). We observed that we obtained a maximum for an imaginary part of the refractive index of $\Im(n_a) = 0.27$.

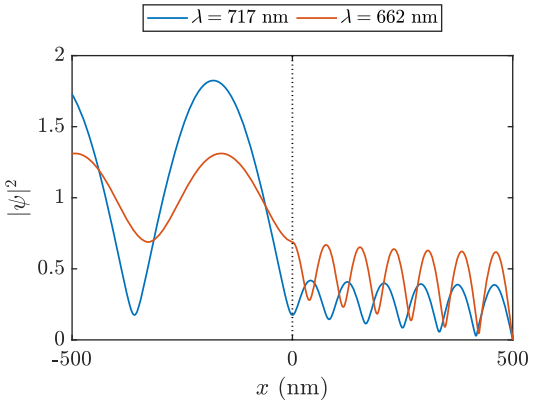

Fig. 3 The wave function in front of and inside the film where a plane wave is propagating from the left toward a single film of thickness 500 nm and refractive index $4.3 + 0.1i$. A perfect mirror is placed behind the film. The system is shown in Fig. 1(c). The wavelength of the plane wave is 717 nm (blue line) and corresponds to a dip, and the wavelength 662 nm (red line) corresponds to a peak in Fig. 2(c) for the case in which the refractive index of the film is $4.3 + 0.1i$.

The thickness of the film was 500 nm, the real part of the refractive index was $\Re(n_a) = 4.3$, and there was a mirror behind the absorptive layer [see Fig. 1(c)]. We consider wave functions for this maximum in the absorption efficiency at $\Im(n_a) = 0.27$. Since the maximum corresponds to a spectral range, we selected wave functions from this range: at 250, 500, and 750 nm for the case in which $n_a = 4.3 + 0.27i$, and the thickness of the absorptive film is 500 nm. Evaluating the wave functions, we found that the optimum of $\Im(n_a)$ is found for the case in which the wave is completely absorbed for small wavelengths and standing waves are present for longer wavelengths. This is shown in Fig. 14.

Until now, we considered absorption enhancement for an absorptive layer of thickness 500 nm, both for different wavelengths and for a total wavelength range. We consider now the absorption properties of layered systems for a changing film thickness. For the film thickness of 500 nm, we found an optimal refractive index of $4.3 + 0.27i$. Figure 4 shows how the absorption efficiency is affected by changing the thickness of the film. The pattern of the absorption efficiency as a function of the wavelength is shown for several film thicknesses in Fig. 4(a). It changes strongly when the film thickness is changed. The strong changes occur since the standing waves occur only when a multiple of the wavelength matches the thickness of the film.

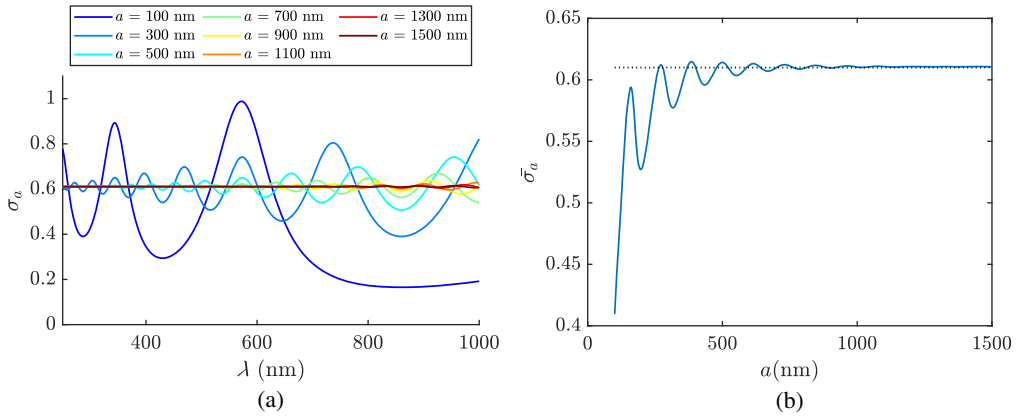

Fig. 4 (a) The absorption efficiency, σ_a, as a function of the wavelength, λ, for a system consisting of a single film with a mirror behind [Fig. 1(c)]. The thickness of the film, a_a, is increased from 100 nm (dark blue line) to 1500 nm (dark red line). The refractive index of the film is $n = 4.3 + 0.27$. (b) The averaged absorption efficiency for the same system as a function of film width.

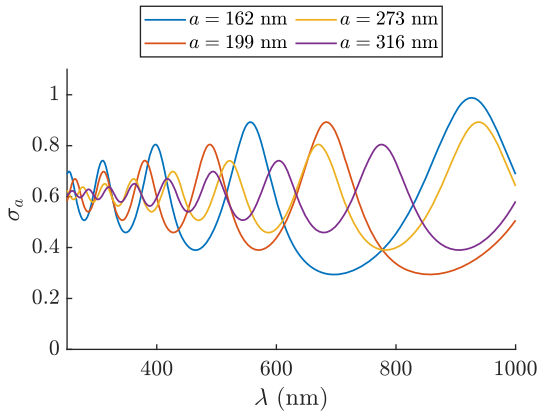

Fig. 5 The absorption efficiency as a function of wavelength for a single film with a refractive index $n = 4.3 + 0.27i$. The thickness of the film is changed and corresponds to the two first peaks ($a = 162$ nm and $a = 273$ nm) and two first dips ($a = 199$ nm and $a = 316$ nm) from the left in $\overline{\sigma}_a(a)$ in Fig. 4(b).

This creates oscillations in the average absorption efficiency $\overline{\sigma}_a(a_a)$, which is plotted as a function of the wavelength [Fig. 4(b)].

We now investigate how the peaks and dips in the average absorption efficiency in Fig. 4(b) are related to the appearance and disappearance of standing waves in the film as a function of the film thickness. We consider two peaks and two dips in the average absorption efficiency in Fig. 4(b), namely the peaks $a = 162$ nm and $a = 273$ nm and the dips at $a = 199$ nm and $a = 316$ nm. In Fig. 5, the corresponding absorption efficiencies are shown for the whole wavelength region. We observe that at thicknesses that correspond to peaks $a = 162$ nm (blue line) and $a = 273$ nm (yellow line) correspond to the cases in which the thicknesses is just large enough that a new resonance is included into the $\sigma_a(\lambda)$ range considered. The thicknesses that correspond to dips, $a = 199$ nm and $a = 316$ nm (red and purple line) correspond to the cases in which the thickness is just large enough that an antiresonance is included.

3.2 *Two Films with Mirror*

To come closer to a real solar cell device, a system consisting of two films and a mirror, as shown in Fig. 1(d), was investigated. The first film is a nonabsorptive layer with a refractive index n_I and a thickness a_I. The refractive index n_I in this layer was set to 1.9, which is the refractive index of ITO at 500 nm, as presented in Ref. 19.

To evaluate how the resonances in the front layer affect the absorption efficiency, two cases were evaluated: (i) a two-film system in which the absorptive film has a thickness that is small enough that light is not completely absorbed in this layer and that resonances can occur and (ii) a two-film system in which all of the light is absorbed in the second layer before it reaches the mirror. The refractive index of the second layer is chosen to be $4.3 + 0.1i$, and the thicknesses are chosen to be (i) 500 nm and (ii) 5000 nm.

To evaluate the resonance structure of the first layer, we consider the integral of the absolute square of the wave function ($|\psi_I(x)|^2$) in the first film according to

$$I_I = \frac{1}{a_I}\int_0^{a_I} |\psi_I(x)|^2 \mathrm{d}x, \tag{4}$$

where a_I is the thickness of the first film and ψ_I is the wave function of the first layer. (The expression for the wave function is given in Table 1.) We refer to the integral over I_I as the total intensity of the wave function $\overline{I}_I$. We start by evaluating case (i), i.e., the absorbing layer has a thickness of 500 nm and light is not completely absorbed by the absorbing layer such that resonances can occur in the absorbing layer. The absorption efficiency as a function of the wavelength $\sigma_a(\lambda)$ for this system is shown in Fig. 6(a) for different thicknesses of the first layer. The averaged absorption efficiency $\overline{\sigma}_a$ for the same system as a function of the thickness of

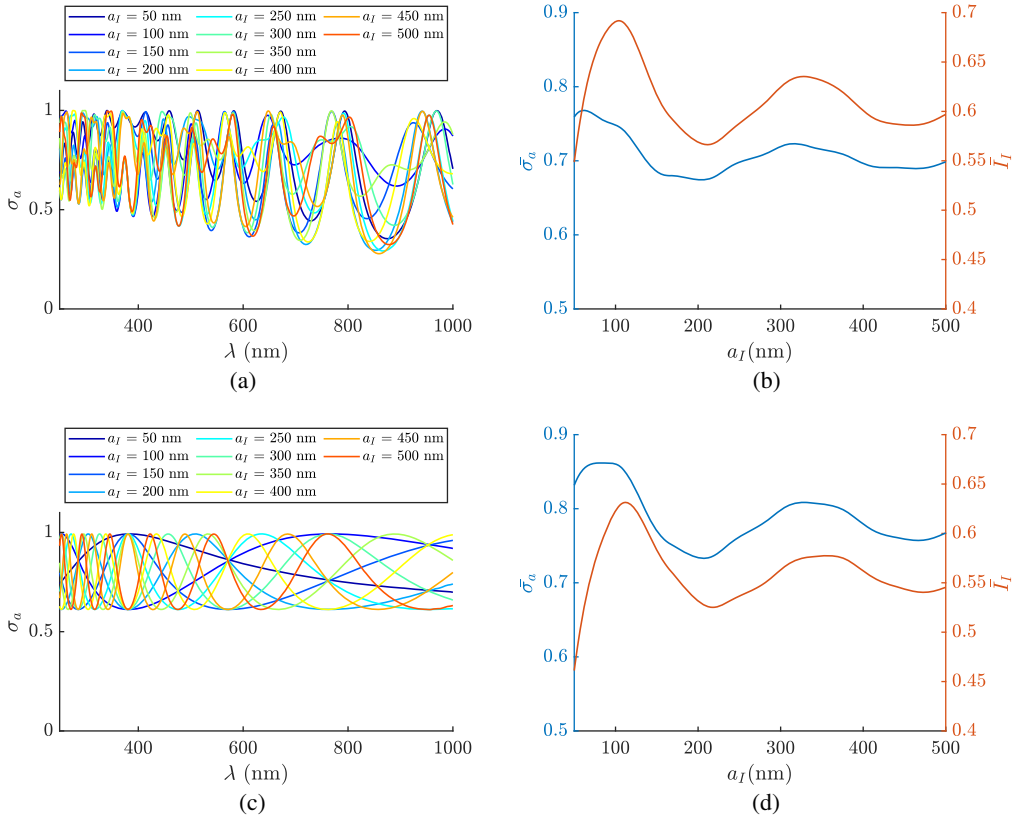

Fig. 6 (a) The absorption efficiency is plotted as a function of the wavelength for a system consisting of two films with a mirror behind. The thickness of the first film is increased from 50 to 500 nm and has a refractive index of 1.9. The second film has a thickness of 500 nm and a refractive index equal to $4.3 + 0.1i$. (b) The averaged absorption efficiency as a function of a_I for the same system. (c), (d) The same plots for a system in which the thickness of the absorptive layer is 5000 nm.

the first layer is shown as the blue line in Fig. 6(b). We compare now the averaged absorption efficiency $\overline{\sigma}_a$ in the absorbing layer with the total intensity of the wave function in the nonabsorbing layer to understand if resonances in the nonabsorbing layer have an effect on the absorption efficiency of the absorbing layer. The red line in Fig. 6(b) shows the integral of the absolute square of the wave function ($|\psi_I(x)|^2$) [see Eq. (4)] averaged with respect to the wavelength, i.e., the total intensity of the wave function in the nonabsorbing layer, $\overline{I}_I$. The units are shown at the right y axis, which is labeled by $\overline{I}_I(a_I)$. Both the red and the blue lines follow the same trend, showing that resonances in the nonabsorbing layer lead to an increase of the absorption efficiency in the absorbing layer. This is the same phenomenon as described, i.e., in the field of optical processes in microcavities, in which it is well known that the life time of resonances is finite due to evanescent leakage.[20]

In the case of a thick totally absorbing second layer with $a_a = 5000$ nm, we observe the same tendency as for the thin absorbing layer: Figs. 6(c) and 6(d) are the plots that correspond to Figs. 6(a) and 6(b), respectively, but this time for case (ii), i.e., a thick absorbing layer with $a_a = 5000$ nm. Figure 6(c) shows the absorption efficiency $\sigma_a(\lambda)$ for the case in which all of the light entering the absorptive film is absorbed. The absorption efficiency $\sigma_a(\lambda)$ is less oscillatory compared with the corresponding graphs for the thin absorbing film in Fig. 6(a). The reason for this is that, in the case of total absorption in the second layer, the resonances are only generated in the nonabsorbing layer. Figure 6(d) shows the average absorption efficiency $\overline{\sigma}_a(a_I)$, as before, as the blue line with units on the left y axis and the total intensity of the wave function $\overline{I}_I(a_I)$ as the red line and units on the right y axis. Again, we observe that the increased

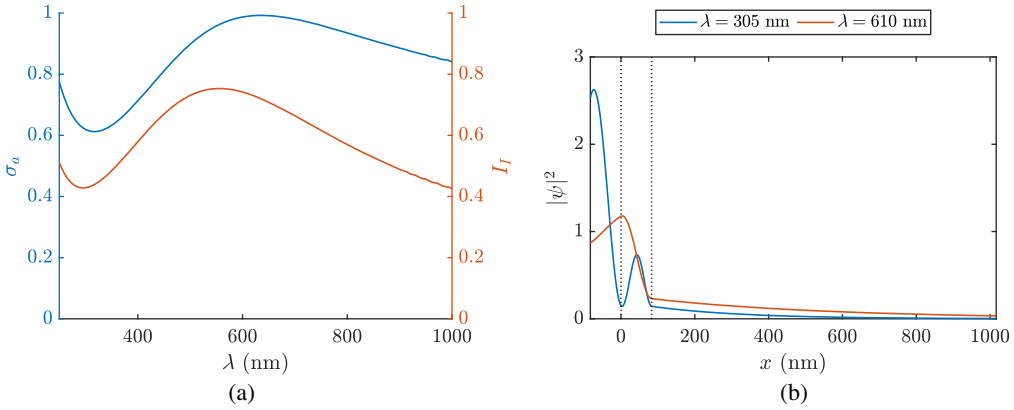

Fig. 7 (a) The absorption efficiency (σ_a) and the integral over the absolute square of the wave function ($|\psi_I(x)|^2$) in the first film (I_I) as a function of wavelength for a system consisting of two films and a mirror behind. The refractive index of the second film is $4.3 + 0.1i$ and the thickness is 5000 nm, i.e., all of the light is absorbed before it reaches the mirror. The first film has a refractive index of 1.9 and a thickness of 83 nm. This thickness corresponds to a maximum in $\overline{\sigma}_a(a_I)$ in Fig. 6(d). A maximum in $\overline{\sigma}_a(a_I)$ is associated with an enhancement of the absorption in the absorbing layer. (b) The absolute square of the wave function for the system for a wavelength corresponding to a top and a dip in panel (a), respectively. The wave function is shown for the nonabsorbing layer and for the first 1000 nm of the absorbing layer, which is 5000 nm thick.

field in the nonabsorbing layer leaks into the absorbing layer and creates an enhanced absorption efficiency.

We now have a closer look at the system with two layers and a mirror with the totally absorbing layer for the situation in which the absorption in the absorbing layer is enhanced by the resonances in the first layer. Inspecting the graph of $\overline{\sigma}_a$ in Fig. 6(d) (blue line), we see that the absorption properties are enhanced for low thicknesses of the nonabsorbing layer. We select the thickness of $a_I = 83$ nm, which leads to an enhancement. In Fig. 7, the absorption efficiency $\sigma_a(\lambda)$ is plotted as a function of the wavelength for the maximum of $\overline{\sigma}_a$ at $a_I = 83$ nm as the blue line with units on the left y axis. The corresponding intensity of the wave function I_I is plotted as a function of the wavelength λ as the red line with units on the right y axis. We see that the absorption efficiency $\sigma_a(\lambda)$ and the intensity of the wave function $I_I(\lambda)$ have a minimum and a maximum in the wavelength range considered, which can be further investigated. The absolute squares $|\psi|^2$ of the wave functions that correspond to the maximum and minimum, respectively, are shown in Fig. 7(b) for the nonabsorbing film and the first 1000 nm of the absorbing film. The wavelengths of the wave function corresponding to the minimum and the maximum were selected to be (i) 305 nm, showing a dip in $\sigma_a(\lambda)$ in Fig. 7(a) (blue line), and (ii) 610 nm, showing a peak in $\sigma_a(\lambda)$ (red line). We observe that, for the case in which the wavelength corresponds to a dip $\sigma_a(\lambda)$ in Fig. 7(a) (blue line), $|\psi|^2$ has lower values in the absorptive film than for the case in which the wavelength corresponds to a peak in $\sigma_a(\lambda)$.

3.3 *Coupling of Resonances of Nonabsorptive Layers*

When the systems consist of three layers, two nonabsorptive layers and an absorptive layer, we can investigate the coupling of resonances in the two nonabsorbing layers. This is the 1D equivalent to a thin-film solar cell with coupling of, e.g., nanospheres on its surface. The coupling of resonances in spherical nanostructures on thin-film solar cells has been discussed in the literature as a cause for enhancement of absorption in the absorbing layers below.[5,6] We start by evaluating how the thicknesses and refractive indices of two nonabsorbing front layers of different materials affect the absorption in the third, absorptive layer. The system is shown in Fig. 1(e). As for the two-film systems, we assume that the refractive indices of the films are constant for all wavelengths. This is to highlight the effect of the thickness of the first two layers on the average of the absorption efficiency, σ_a. The thickness of the third, absorptive film is chosen such that the wave function in this film is totally absorbed.

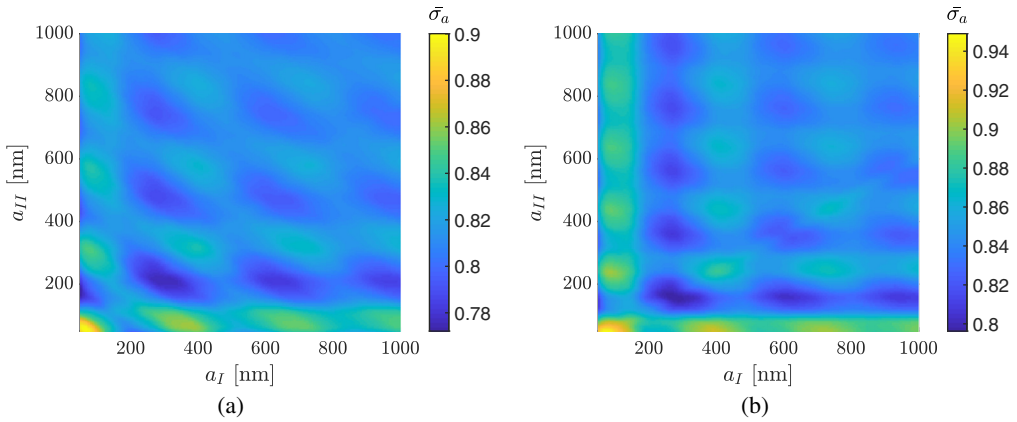

Fig. 8 The average absorption efficiency, $\overline{\sigma}_a$, for a three-layer system as shown in Fig. 1(e) is displayed as a heat map for varying thicknesses of the two first nonabsorbing layers. The thicknesses of the two first layers were varied between 50 and 1000 nm. The thickness of the third layer was kept constant at 5000 nm. The refractive indices of the layers are: (a) $n_I = 1.5$ (refractive index of SiO_2 at 500 nm), $n_{II} = 1.9$ (refractive index of ITO at 500 nm), and $n_{III} = 4.3 + 0.01i$ (where the real part of n_{III} is the real part of the refractive index of Si at 500 nm and the imaginary part of n_{III} is chosen so that all light that enters the absorptive film is absorbed. (b) The refractive indices are given as $n_I = 1.5$, $n_{II} = 2.5$ (selected to be substantially above n_I), and $n_{III} = 4.3 + 0.01i$. The wavelength range that is investigated is 250 to 1000 nm.

In Fig. 8(a), the average absorption efficiency is shown for the three-film system, in which the refractive indices of layers I, II, and III in Fig. 1(e) are set to 1.5 (refractive index of SiO_2 at 500 nm), 1.9 (refractive index of ITO at 500 nm), and $4.3 + 0.01i$, respectively. The thickness of the third layer is set to 5000 nm, i.e., all light that enters the third layer is absorbed. The thicknesses of the two first layers in the system were varied between 50 and 1000 nm to optimize the thicknesses of the two films with respect to the absorption efficiency of the third film. Figure 8(a) shows $\overline{\sigma}_a$ for different combinations of the thicknesses of the two first layers. We consider the wavelength range from 250 to 1000 nm. In Fig. 8(b), the corresponding results for the same system with an increased refractive index of the second layer are shown. The refractive indices of the layers I, II, and III are now set to 1.5, 2.5, and $4.3 + 0.01i$, respectively. As before, the wavelength range is evaluated in the region 250 to 1000 nm. The thicknesses of the two first layers are changed between 50 and 1000 nm, and the thickness of the third layer is 5000 nm. A comparison between Figs. 8(a) and 8(b) shows that, in the case in which the two first layers have relatively close refractive indices, the pattern in the heat map is a skewed grid pattern, while in Fig. 8(b) a nonskewed grid pattern is obtained. When the refractive indices of the two first layers are at a similar level, the resonances couple and the grid pattern is skewed. In the case in which the difference between the refractive indices in the two layers is large, the resonances in the layers are independent of each other, and the grid pattern of $\overline{\sigma}_a$ is not skewed.

To evaluate the coupling of the resonances further, we consider the three-layer system shown in Fig. 1(f) in which the first and third layers are the nonabsorptive layers and the second layer is the absorptive layer. The back side mirror is removed to avoid the effect of an increased σ_a caused by all light being forced to travel back and forth in the third film.

In Figs. 9(a) and 9(b), the averaged absorption efficiency, $\overline{\sigma}_a$, is shown as a heat map as a function of the thickness of the nonabsorptive layers, a_I and a_{III}. For the system in Fig. 9(a), the refractive indices of the layers I, II, and III are wavelength independent, as before, and set to 1.9, $4.3 + 0.1i$, and 1.5, respectively. The thickness of the absorptive layer is 500 nm.

In Fig. 9(b), the system parameters are identical to the situation shown in Fig. 9(a), except that the refractive index of the third layer is set to 1.9, i.e., the refractive indices of the two nonabsorptive layers are identical. It is, therefore, expected that the resonances in the two nonabsorptive layers occur at the same thicknesses and wavelengths.

The grid patterns observed in Figs. 9(a) and 9(b) indicate that both layers affect $\overline{\sigma}_a$. But the differences are more distinguished for changes of thicknesses of the first layer than of the third.

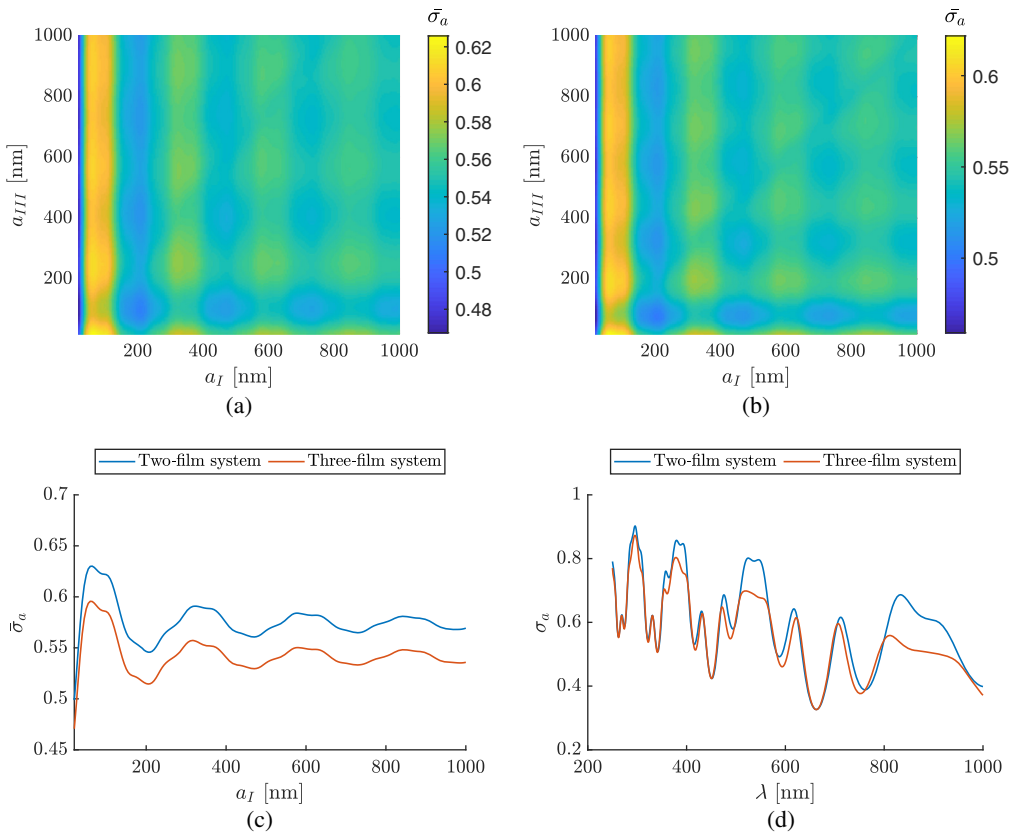

Fig. 9 (a), (b) A heat map of the averaged absorption efficiency $\overline{\sigma}_a$ for a three-film system [see Fig. 1(f)]. The averaged absorption efficiency $\overline{\sigma}_a$ is shown as a function of the thicknesses of the first and third layer a_I and a_{III}. The refractive indices of the layers are: (a) $n_I = 1.9$, $n_a = 4.3 + 0.01i$, and $n_{III} = 1.5$ and (b) $n_I = 1.9$, $n_a = 4.3 + 0.01i$, and $n_{III} = 1.9$, respectively. The thickness of the second layer is 500 nm. (c) The average absorption efficiency $\overline{\sigma}_a$ as a function of a_I for the two- (blue line) and three-film (red line) systems. For both systems, the refractive index of the first layer is set to 1.9 and for the second layer to 4.3 + 0.1. The thickness of the second layer is 500 nm. For the three-film system, the third film has a refractive index of 1.9 and a thickness of 350 nm. (d) $\sigma_a(\lambda)$ for the same systems as in (c) when the thickness of the first layer is 350 nm.

The blue line in Fig. 9(c) shows the averaged absorption efficiency $\overline{\sigma}_a$ as a function of the thickness of the first layer in a two-film system (without a back side mirror), i.e., $n_{III} = 1$ in the system shown in Fig. 1(f). The refractive index of the first layer is 1.5, the refractive index of the second layer is $n_a = 4.3 + 0.1i$, and the thickness of the second layer is 500 nm. The red line shows the averaged absorption efficiency $\overline{\sigma}_a$ as a function of a_I for an equivalent three-film system in which the refractive index of the third layer is $n_{III} = 1.9$ and the thickness of the third film is $a_{III} = 350$ nm. In Fig. 9(d), the absorption efficiencies $\sigma_a(\lambda)$ for the two- and three-film systems are compared as a function of λ. For both systems, the first two layers are identical with thicknesses and refractive indices set to 350 and 500 nm and $n_I = 1.9$ and $n_a = 4.3 + 0.1i$, respectively. For the three-film systems, the refractive index and the thickness of the third film are $n_{III} = 1.9$ and 350 nm, respectively. Both Figs. 9(c) and 9(d) show that a two-film system has a higher absorption efficiency than a corresponding three-layer system with $a_{III} = 350$ nm. This indicates that the coupling of resonances in this case does not have any enhancement effect.

To return to a system that is closer to a real solar cell device, the system in Fig. 1(g) was evaluated to further describe the effect of coupling in the case in which a back side mirror is present. The refractive indices were selected as above, and the three-layer system was compared with an equivalent two-layer system in which the third layer is removed as in Fig. 1(d). Figures 10(a) and 10(b) show the averaged absorption cross section as a function of the thickness of the nonabsorptive layers, a_I and a_{III}. The thickness of the absorptive middle layer is 500 nm.

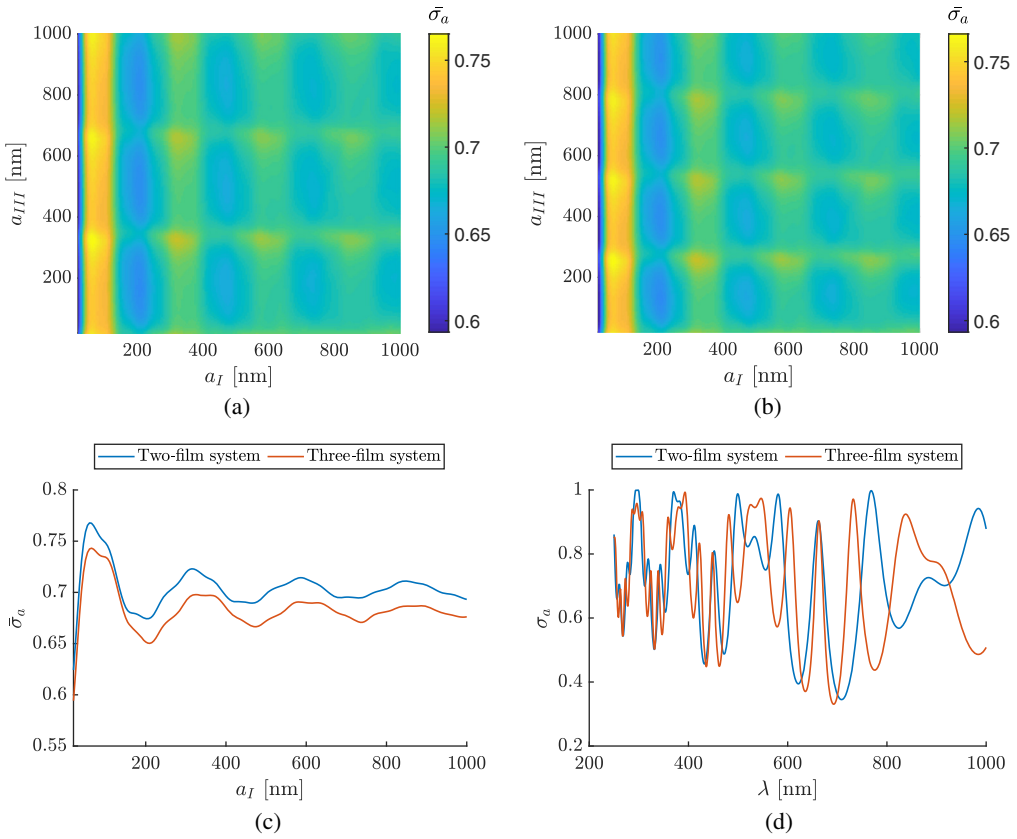

Fig. 10 (a), (b) A heat map of the averaged absorption efficiency $\overline{\sigma}_a$ for a three-film system with a back side mirror [see Fig. 1(g)]. The averaged absorption efficiency $\overline{\sigma}_a$ is shown as a function of the thicknesses of the first and third layer a_I and a_{III}. The refractive index of the layers are for (a) $n_I = 1.9$, $n_{II} = 4.3 + 0.01i$, and $n_{III} = 1.5$ and (b) $n_I = 1.9$, $n_{II} = 4.3 + 0.01i$, and $n_{III} = 1.9$, respectively. The thickness of the second layer is 500 nm. (c) The average absorption efficiency $\overline{\sigma}_a$ as a function of a_I for a two-film system (blue line) and a three-film system (red line). For both systems, the refractive index of the first layer is set to 1.9 and for the second layer to 4.3 + 0.1. The thickness of the second layer is 500 nm. For the three-film system, the third film has a refractive index of 1.9 and a thickness 350 nm. (d) $\sigma_a(\lambda)$ for the same systems as in (c) in which the thickness of the first layer is 350 nm.

The refractive indices are chosen as $n_I = 1.9$, $n_a = 4.3 + 0.1i$, and $n_{III} = 1.5$ for the results shown in Fig. 10(a) and as $n_I = 1.9$, $n_a = 4.3 + 0.1i$, and $n_{III} = 1.9$ for the results shown in Fig. 10(b). We observe that the maximum $\overline{\sigma}_a$ is higher than for the system without a mirror (Fig. 9). This is due to the light being reflected at the mirror on the back side, which was effectively doubling the effective thickness of the absorbing layer. Further, we observe the same trend that we discussed for Fig. 9: adding a third layer with an identical refractive index, which is expected to lead to coupling of resonances, does not enhance $\overline{\sigma}_a$.

The blue line in Fig. 10(c) shows the averaged absorption efficiency $\overline{\sigma}_a$ as a function of the thickness of the first layer in the two-film system [shown in Fig. 1(d)]. The refractive index of the first layer is 1.5, the refractive index of the second layer is $n_a = 4.3 + 0.1i$, and the thickness of the second layer is 500 nm. The red line shows the averaged absorption efficiency $\overline{\sigma}_a$ as a function of a_I for an equivalent three-film system in which the refractive index of the third layer is $n_{III} = 1.9$ and the thickness of the third film is $a_{III} = 350$ nm. We observe that, with the back side mirror present, the third film reduces $\overline{\sigma}_a$. This is the same trend as what we observed for the case without a mirror. Compared with the system without a mirror on the back side in Fig. 9(c), $\overline{\sigma}_a$ is less reduced in the system with a mirror on the back side.

In Fig. 10(d), the absorption efficiencies $\sigma_a(\lambda)$ as a function of λ are compared for the two- and three-film systems. The thicknesses and refractive indices of the two first layers are set to 350 and 500 nm and $n_I = 1.9$ and $n_a = 4.3 + 0.1i$, respectively, for both systems. For the three-

film systems, the refractive index and the thickness of the third film are $n_{III} = 1.9$ and 350 nm, respectively. If the wave function is evaluated in a point with a peak in $\sigma_a(\lambda)$ for the two-film system in Fig. 10(d), e.g., 769 nm, we would observe that $|\psi|^2$ is higher for the two-film system than for the three-film system. The opposite would be observed when selecting a wavelength that corresponds to a peak in the three-film system, e.g., 732 nm. This is shown in Fig. 15.

As predicted by Eq. (3), the absorption efficiency is enhanced when the field in the absorptive material is increased. From Fig. 10(c), we learn that a two-film yields a higher average absorption efficiency. However, as Fig. 10(d) indicates, the absorption efficiency is wavelength-dependent.

However, the result is that coupling of resonances in thin films does not overall increase the absorption efficiency. This can be seen both for two- and three-layer systems with and without a mirror in Figs. 9 and 10, respectively.

3.4 *Optimization of Absorption of Thin-Film Solar Cells*

In this section, we demonstrate how considering resonances in thin-film systems can help to optimize experimentally realizable solar cells. We consider the system shown in Fig. 11(b), which is a simplification of a five-layer epitaxial crystalline silicon solar cell that is optically thin as shown in Fig. 11(a).[19] The experimentally realized system consists of three different materials: ITO, amorphous silicon, and crystalline silicon. The two silicon layers consist of one p-doped and one n-doped layer as shown in the figure. To simplify the system, we treat the amorphous silicon as one layer with the same wavelength-dependent refractive index. The same assumption is used for the crystalline silicon. The absorption efficiency is calculated by Eq. (2). The refractive index of the three layers that are used is experimentally determined.[21–23] By evaluating the absorption efficiency for different choices of thickness for the three layers, the system can be optimized to absorb as much radiation as possible. For the calculation of $\overline{\sigma}_a$, the spectra are weighted by the AM1.5 solar spectrum.

The system in Fig. 11(b) is evaluated for several thicknesses of the layers. The average absorption efficiency $\bar{\sigma}_a$ is shown for systems with c-Si film thickness equal to 0.5, 2, 8, 32, 100, and 200 μm in Fig. 12. The thicknesses of the two first layers are varied between 20 and 500 nm. As Fig. 12 indicates, certain combinations of thicknesses of the two first layers give higher $\overline{\sigma}_a$ values than the others.

As Fig. 12 indicates, 60 and 150 nm are optimal thicknesses for the first and the second layers, respectively. We, therefore, set the thicknesses of the first and second layers to 60 and 150 nm and vary the thickness of the third layer. By continuously increasing the thickness of the third layer from 0.5 to 100 μm, the findings of Sec. 3.2 are confirmed. When the thickness of the energy converting layer is increased, the average absorption efficiency $\overline{\sigma}_a$ stabilizes at a certain value. This is shown in Fig. 13, where the average absorption efficiency $\overline{\sigma}_a$ is shown as a function of the thickness of the third layer when the spectra are weighted by the AM1.5 solar spectrum.[24] We observe that the $\overline{\sigma}_a$ stabilizes at a maximum value of approximately $\overline{\sigma}_a = 0.5$. The

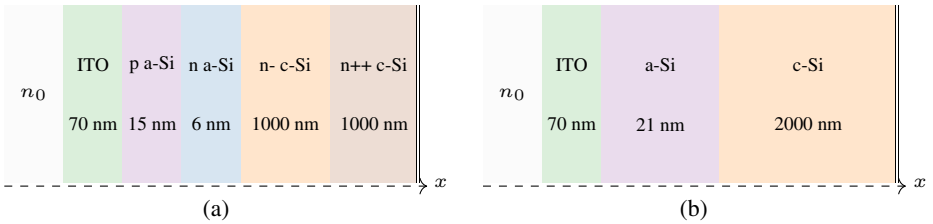

Fig. 11 (a) A multilayer thin-film solar cell, consisting of five thin layers and a mirror. This solar cell has been experimentally realized[19] and consists of ITO, n- and p-doped amorphous and crystalline silicon. The thicknesses of the layers of the experimentally realized system are shown in the model. (b) The system has been simplified into a three-layered system with a mirror.[9] The system has been simplified by replacing the layers having different doping with one single layer with the experimentally determined refractive index.[21–23] n_0 indicates the refractive index of vacuum and is given by $n_0 = 1$. Behind the layers of the different materials, a perfect mirror is placed. To optimize the system, the thicknesses of the three layers are changed. The result is shown in Fig. 12.

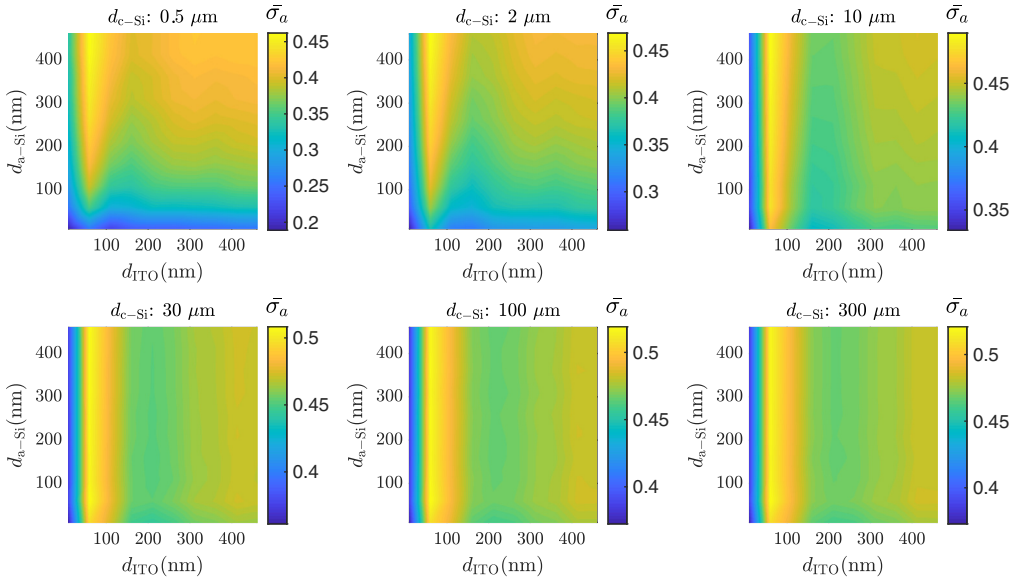

Fig. 12 The average absorption efficiency $\overline{\sigma}_a$ for a three-film system with the same materials as shown in Fig. 11(b) with experimentally determined refractive indices.[21–23] The thicknesses of the two first layers are varied between 20 and 500 nm. The thickness of the c-Si layer is set to 0.5, 2, 10, 30, 100, 200, and 300 μm, respectively. The wavelength range that is investigated is from 250 to 1000 nm. The spectra are weighted by the AM1.5 solar spectrum.[24]

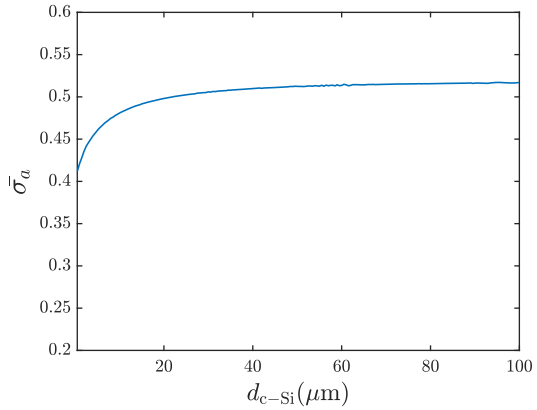

Fig. 13 The average absorption efficiency, $\overline{\sigma}_a$, as a function of the thickness of the c-Si layer. The system is equivalent to the system shown in Fig. 11(b) with the thicknesses of ITO and a-Si set to 60 and 150 nm, respectively. Further, the thickness of the c-Si layer, d_{c-Si}, is increased from 0.5 to 200 μm. The refractive indices of the layers are experimentally determined.[21–23] The spectra are weighted by the AM1.5 solar spectrum.[24]

stabilization takes place when the thickness of the third layer is ~50 μm. For larger thicknesses, no further enhancement of the absorption of the c-Si layer can be obtained. A further investigation of the material cost versus the absorption efficiency is needed to decide if a thickness of 50 μm is an optimum because a thickness of the c-Si layer of around 20 μm is close to the optimum value for the average absorption efficiency $\overline{\sigma}_a$.

4 Discussion

The results presented in Sec. 3.1 show that, when the imaginary part of the refractive index of the absorptive material is changed, the resonance structure of the absorption efficiency and the

absorption properties of the material change. For a large imaginary part of the refractive index, all radiation entering the absorptive material is absorbed before it reaches the back side boundary or mirror. Therefore, standing waves do not occur in the absorptive material for a large imaginary part of the refractive index. One might assume an increasing imaginary part of the refractive index results in an increased absorption efficiency. However, as confirmed by the Fresnel equations,[14] the reflection from the absorbing film's surface increases when the imaginary part of the refractive index increases. Therefore, less radiation is transmitted into the absorptive material, which results in lower absorption. As Figs. 2(d) and 2(f) show, there is an optimal size of the imaginary part of the refractive index of the absorptive material, with the wave function being just totally absorbed before it reaches the mirror. Since we consider the average absorption efficiency for a whole wavelength region, this condition of optimal imaginary part of the refractive index is achieved, with the standing wave in the absorbing material just disappearing for small wavelengths, while it is present for large wavelengths (this is shown in the Appendix). When investigating the absorption properties of the film system as a function of the thickness of the absorbing film, we observe that the absorption increases with increasing thickness of the absorbing layer until a maximum is reached and stays constant for larger thicknesses. Before we reach this point, the average absorption efficiency $\bar{\sigma}_a$ oscillates as shown in Fig. 4. The peaks of the oscillatory pattern correspond to a thickness of the absorptive material that includes a new resonance, while the dips correspond to a thickness of the absorptive material that includes a new antiresonance. This mechanism can be potentially used to enhance absorption efficiency of thin-film solar cells within a desired wavelength range. In general, we see that absorption in the absorbing layer is enhanced by resonances in the nonabsorptive material, which lead to a field enhancement in the absorbing material. This is shown in Sec. 3.2. In this section, we also learn that the resonance in the absorption efficiency follows the same trend as the averaged integral over the nonabsorptive film. An increase in the integral over the absolute square of the wave function is followed by an increased $\sigma_a(\lambda)$.

When considering a system consisting of three layers, we find that it is important to investigate first all combinations of thicknesses of the first two layers to optimize the thicknesses. The optimal thickness of the third layer is then found, with the wave function being just totally absorbed.

A three-film system without a mirror is also considered to evaluate the effect of coupling between two nonabsorptive films on each side of the absorptive film. From Figs. 9(a) and 9(b), we conclude that mainly the resonances in the front layer affect the averaged absorption efficiency $\overline{\sigma}_a$. When we compare the two- and three-film systems without a back side mirror in Figs. 9(c) and 9(d), we observed that the absorption efficiency was lower for the three-film system. This can be understood when considering that the refractive index changes at the boundary. The refractive index in the third film is closer to the refractive index of air at the outside, which results in more light being transmitted out of the system. This is expected from Fresnel's equations. We further investigated a three-layer system with the absorbing layer in the middle and a mirror on the back side to avoid more leakage of radiation from the third film to the outside. Strikingly, also in the case of a three-film system with a mirror on the back side, the absorption efficiency was not increased compared with the corresponding two layer-system without the third nonabsorbing layer. The results are shown in Fig. 10. This indicates that the coupling of resonances itself is not a mechanism that increases the absorption efficiency of solar cells in the layered system. Coupling of resonances has been suggested as a mechanism for resonance enhancement in surface-structured thin-film solar cells.[5,6] We would, therefore, expect that, when spheres are embedded into the energy-converting material,[25] it is rather the field enhancement due to resonances in each sphere than the coupling of the resonances that would lead to an absorption enhancement.

In Sec. 3.4, the absorption efficiencies for experimentally realizable thin-film solar cells are investigated. An experimentally realized solar cell was used as a template, and wavelength-dependent, experimentally determined refractive indices were used in the system. The observations were comparable to the results found in Sec. 3.1, in which systems with wavelength-independent refractive indices are investigated.

In all systems considered, we studied the average absorption efficiency, $\overline{\sigma}_a$. It is important to note that $\overline{\sigma}_a$ changes if we change the wavelength range. It is therefore essential to optimize the system according to the proper wavelength range. In our study, the results presented, except Sec. 3.4, were not weighted with the solar spectrum. If the absorption efficiency is multiplied with the solar spectrum, the optical generation rate[9,12] is obtained.

Our model is exact for situations with coherent light, which is a common assumption for simulations of thin-film solar cells in which the thickness of the films is smaller than the coherence wavelength.[26] Sunlight, however, is incoherent, so the assumption of coherent light in our model is not strictly applicable to the case of incoherent sunlight. Indeed, it is known that there is a difference in conversion efficiency between illumination with coherent and incoherent light.[27] Since the spatial coherence area of sunlight is about 60 μm $\times$ 60 μm,[28] and resonant solar-cell surface structures are on the order of a micron, the effects of spatial coherence may be neglected. However, since the temporal coherence length of sunlight is about 600 nm,[29] and the thicknesses of our films are about on this order of magnitude, the temporal incoherence of sunlight cannot be neglected. Therefore, while our results are rigorous for coherent incident light, we have to be careful when using these results to make predictions for the case of incoherent sunlight. On the upside, a two-step method that takes the results of coherent calculations as input for a folding step that then obtains conversion efficiencies for incoherent illumination directly from the coherent input exists.[27,30] Therefore, our results presented here are the first step in this two-step process. The investigation of our systems for the use of incoherent light is beyond the scope of this study and will be addressed in a follow-up work.

For monochromatic light, our results indicate that the optimum in conversion efficiency is reached when the layers in front of the energy-converting material are around the same size as the coherence length of the natural sunlight.[29] We could, therefore, expect resonances in the first layers. Further, we show that it is optimal that the energy-converting material should have a thickness so that the wave function is totally absorbed before it reaches the mirror. In these cases, we will not have resonances in the layer closest to the mirror. We expect that these predictions, based on a coherent, monochromatic model, are robust and will hold in the case of illumination with incoherent light.

Our model only evaluates the optical properties of the system. Effects linked to losses other than reflection are not included.

5 Conclusions

In this paper, we have shown that simple calculations of the absorption efficiency can give an indication of a proper choice of thickness of the layers in a thin-film solar cell. We find that a resonance in the front layers can result in an increased absorption efficiency. This is caused by the enhanced wave function in the front layers. Due to the continuity of the wave function, this also results in an enhanced absorption of radiation in the absorptive material. In the case of a nonabsorptive layer on both sides of the absorptive layer, the resonances in the first layer are the most important. We investigated further if the coupling of resonances could enhance absorption in an absorptive layer that was located between absorbing layers and could not find any effect.

We have also shown that the absorption efficiency decreases when the imaginary part of the refractive index of the absorptive material increases. This is because the reflection probability increases according to Fresnel's equations. An optimal imaginary part of the refractive index is therefore obtained when the absorption is high enough such that standing waves just disappear in the absorbing material for a large part of the wavelength region considered, but not so high that a large part of the radiation is not reflected in the energy-converting material. We have applied our findings with success to the optimization of an experimentally realizable solar-cell system.

The results and methods presented in this paper are directly transferable to the case of oblique incidence.[13] Oblique incidence results in a shift of the resonances in the wavelength range, i.e., the same techniques presented in this paper can be used for oblique incidence.

6 Appendix: Investigation of Resonance Structures in Optically Thin-Solar Cells

6.1 *Wave Function of Layered Film Systems*

The systems shown in Fig. 1 with normal incident light can be described by the exact scalar wave theory. We set the first boundary from the left for the systems shown in Fig. 1 at $x = 0$ and obtain the wave functions given in Table 1. The amplitudes of the wave functions in Table 1 can be found by requiring that the wave functions and their first derivatives are continuous across the boundary.[15]

6.2 $|\psi|^2$ *for a Single Film for Increasing Wavelengths*

Figure 14 shows the absolute square of the wave function for a system consisting of a single film with a mirror behind for increasing wavelengths. The refractive index of the film is $4.3 + 0.27i$, and the thickness of the film is 500 nm. The figure shows how the resonance structure is kept for the long wavelengths but not for the very long wavelengths.

6.3 *Comparison of* $|\psi|^2$ *for Two- and Three-Film Systems*

In Fig. 15, the absolute square of two selected wave functions is shown for the two- and three-film systems. For the two-film system with the mirror on the back side [see Fig. 1(d)], the wave function is plotted as a blue line in Fig. 15. As for the case without a mirror, we chose $a_I = 350$ nm and $a_a = 500$ nm. For the three-film systems with the mirror placed behind the third

Table 1 Wave functions for the systems shown in Fig. 1. The first boundary from the left is assumed to be at $x = 0$. The amplitude of the incoming plane wave is 1, r is the amplitude of the reflected wave, and t is the amplitude of the transmitted wave. A, B, C, D, E, and F are amplitudes of the wave functions inside the films. k is the angular wave number given by $k = \frac{2\pi}{\lambda}$. n_I, n_{II}, n_{III}, and n_a are the refractive indices, and a_I, a_{II}, a_{III}, and a_a are the thicknesses of the films as indicated in the figure.

System	Wave function
System a [Fig. 1(a)]	$\psi_a(x) = \begin{cases} e^{ikx} + re^{-ikx} & \text{for } x < 0 \\ Ae^{in_a kx} & \text{for } x > 0 \end{cases}$
System b [Fig. 1(b)]	$\psi_b(x) = \begin{cases} e^{ikx} + re^{-ikx} & \text{for } x < 0 \\ Ae^{in_a kx} + Be^{-in_a kx} & \text{for } 0 < x < a_a \\ te^{ikx} & \text{for } x > a_a \end{cases}$
System c [Fig. 1(c)]	$\psi_c(x) = \begin{cases} e^{ikx} + re^{-ikx} & \text{for } x < 0 \\ A\sin(n_a k(x - a_a)) & \text{for } 0 < x < a_a \end{cases}$
System d [Fig. 1(d)]	$\psi_d(x) = \begin{cases} e^{ikx} + re^{-ikx} & \text{for } x < 0 \\ Ae^{in_I kx} + Be^{-in_I kx} & \text{for } 0 < x < a_I \\ C\sin(n_a k(x - (a_I + a_a))) & \text{for } a_I < x < (a_I + a_a) \end{cases}$
System e [Fig. 1(e)]	$\psi_e(x) = \begin{cases} e^{ikx} + re^{-ikx} & \text{for } x < 0 \\ Ae^{in_I kx} + Be^{-in_I kx} & \text{for } 0 < x < a_I \\ Ce^{in_{II} kx} + De^{-in_{II} kx} & \text{for } a_I < x < (a_I + a_{II}) \\ E\sin(n_a k(x - (a_I + a_{II} + a_a))) & \text{for } (a_I + a_{II}) < x < (a_I + a_{II} + a_a) \end{cases}$
System f [Fig. 1(f)]	$\psi_f(x) = \begin{cases} e^{ikx} + re^{-ikx} & \text{for } x < 0 \\ Ae^{in_I kx} + Be^{-in_I kx} & \text{for } 0 < x < a_I \\ Ce^{in_a kx} + De^{-in_a kx} & \text{for } a_I < x < (a_I + a_a) \\ Ee^{in_{III} kx} + Fe^{-in_{III} kx} & \text{for } (a_I + a_a) < x < (a_I + a_a + a_{III}) \\ te^{ikx} & \text{for } x > (a_I + a_a + a_{III}) \end{cases}$
System g [Fig. 1(g)]	$\psi_g(x) = \begin{cases} e^{ikx} + re^{-ikx} & \text{for } x < 0 \\ Ae^{in_I kx} + Be^{-in_I kx} & \text{for } 0 < x < a_I \\ Ce^{in_a kx} + De^{-in_a kx} & \text{for } a_I < x < (a_I + a_a) \\ E\sin(n_{III} k(x - (a_I + a_a + a_{III}))) & \text{for } (a_I + a_a) < x < (a_I + a_a + a_{III}) \end{cases}$

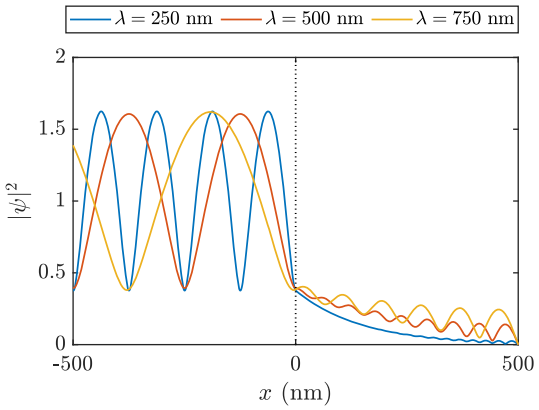

Fig. 14 The absolute square of the wave function for a system consisting of an absorptive film with a thickness of 500 nm and a refractive index equal to $4.3 + 0.27i$. This value of the imaginary part of the refractive index was to be the optimum in the average absorption efficiency in Fig. 2(f).

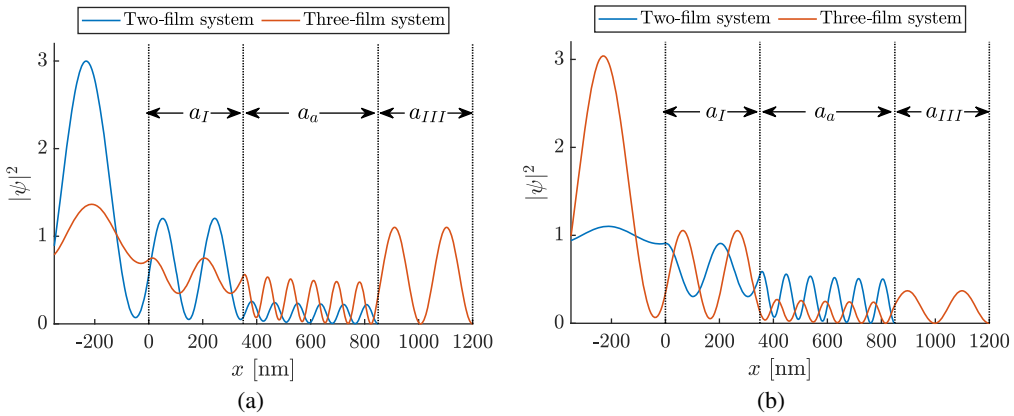

Fig. 15 The absolute square of the wave functions (given in Table 1) as a function of position. The thicknesses is selected to be $a_I = 350$ nm, $a_a = 500$ nm, and $a_{III} = 350$ nm, and the refractive indices are $n_I = 1.9$, $n_{II} = 4.3 + 0.01i$, and $n_{III} = 1.9$. The blue line shows $|\psi|^2$ for the two-film system [Fig. 1(d)], with the back side mirror placed behind the absorptive film of thickness a_a. The red line shows $|\psi|^2$ for a three-film system [Fig. 1(g)], with the back side mirror placed behind the third, nonabsorptive layer of thickness a_{III}. (a) The behavior of the wave function in the case in which the wavelength of the incoming light is 732 nm [corresponding to second peak from right in Fig. 10(d) for the three-film system]. (b) The behavior of the wave function in the case in which the wavelength of the incoming light is 769 nm [corresponding to second peak from right in Fig. 10(d) for the two-film system].

film [see Fig. 1(g)], $a_I = 350$ nm, $a_a = 500$ nm, and $a_{III} = 350$ nm. The refractive indices are selected to be $n_I = 1.9$, $n_{II} = 4.3 + 0.01i$, and $n_{III} = 1.9$, respectively. The parameters are again chosen analog to the system without a mirror. The wavelength of the incoming plane wave is selected to be 732 nm in Fig. 15(a). This wavelength corresponds to the second peak from the right in Fig. 10(d) for the three-film system. In Fig. 15(b), the wavelength is selected to be 769 nm. This corresponds to the second peak from the right in Fig. 10(d) for the two-film system. The wave functions in Fig. 15 confirm Eq. (3) that, when the absolute square of the wave function $|psi|^2$ has increased absolute values in the absorptive film, increased absorption efficiency is obtained. For the selected wavelength of the incoming plane wave in Fig. 15(a), σ_a is larger for the three-film system than for the two-film system and $|\psi(x)|^2$ is larger for the three-film system (red line) than for the two-film system (blue line). In Fig. 15(b), the selected wavelength corresponds to a peak in σ_a for the two-film system, and $|\psi(x)|^2$ is larger for the two-film system (blue line) than for the three-film system (red line).

Acknowledgments

This work was supported by the grant "Development of a new ray model for understanding the coupling between dielectric spheres for photovoltaics with higher efficiency" (Grant No: 250678), financed by the Research Council of Norway. We thank Dr. Tor Nordam for valuable input in the final phase of the writing process. The authors declare that they have no known competing financial interests or personal relationships that could appear to have influenced the work reported in this paper.

References

1. R. Brendel, *Thin-Film Crystalline Silicon Solar Cells: Physics and Technology*, John Wiley & Sons, Weinheim, Germany (2003).
2. T. D. Lee and A. U. Ebong, "A review of thin film solar cell technologies and challenges," *Renewable Sustainable Energy Rev.* **70**, 1286–1297 (2017).
3. J. Grandidier et al., "Light absorption enhancement in thin-film solar cells using whispering gallery modes in dielectric nanospheres," *Adv. Mater.* **23**(10), 1272–1276 (2011).
4. G. Kang et al., "Broadband light-trapping enhancement in an ultrathin film a-si absorber using whispering gallery modes and guided wave modes with dielectric surface-textured structures," *Adv. Mater.* **25**(18), 2617–2623 (2013).
5. C. Becker et al., "5×5 cm^2 silicon photonic crystal slabs on glass and plastic foil exhibiting broadband absorption and high-intensity near-fields," *Sci. Rep.* **4**, 5886 (2015).
6. M. Schmid, "Review on light management by nanostructures in chalcopyrite solar cells," *Semicond. Sci. Technol.* **32**(4), 043003 (2017).
7. H. ElAnzeery et al., "Refractive index extraction and thickness optimization of $Cu_2ZnSnSe_4$ thin film solar cells," *Phys. Status Solidi A* **212**(9), 1984–1990 (2015).
8. S. Saylan et al., "Multilayer antireflection coating design for $GaAs_{0.69}/P_{0.31}$/Si dual-junction solar cells," *Sol. Energy* **122**, 76–86 (2015).
9. M. Brandsrud et al., "Exact ray theory for the calculation of the optical generation rate in optically thin solar cells," *Physica E* **105**, 125–138 (2019).
10. H. C. Hulst and H. C. van de Hulst, *Light Scattering by Small Particles*, Courier Corporation, New York (1981).
11. E. Seim et al., "Chaos: a new mechanism for enhancing the optical generation rate in optically thin solar cells," *Chaos* **29**(9), 093132 (2019).
12. V. E. Ferry, J. N. Munday, and H. A. Atwater, "Design considerations for plasmonic photovoltaics," *Adv. Mater.* **22**(43), 4794–4808 (2010).
13. M. A. Brandsrud et al., "An exact ray model for oblique incident light on planar films," *Physica E* **126**, 114374 (2021).
14. M. N. Sadiku, *Elements of Electromagnetics*, 5th ed., international ed.,Oxford University Press, New York (2014).
15. J. Townsend, *Quantum Physics: A Fundamental Approach to Modern Physics*, University Science Books, California (2010).
16. D. J. Griffiths, *Introduction to Electrodynamics*, 3rd ed., Prentice Hall, Upper Saddle River, New Jersey (1999).
17. D. Cozza et al., "Optical modeling and optimizations of $Cu_2ZnSnSe_4$ solar cells using the modified transfer matrix method," *Opt. Express* **24**(18), A1201–A1209 (2016).
18. P. A. Tipler and G. Mosca, *Physics for Scientists and Engineers: With Modern Physics*, 6th ed., Freeman, New York (2008).
19. J. K. Selj, D. Young, and S. Grover, "Optimization of the antireflection coating of thin epitaxial crystalline silicon solar cells," *Energy Procedia* **77**, 248–252 (2015).
20. J. U. Nöckel and A. D. Stone, *Chaotic Light: A Theory of Asymmetric Resonant Cavities*, pp. 389–426, World Scientific (1996).
21. M. A. Green, "Self-consistent optical parameters of intrinsic silicon at 300 k including temperature coefficients," *Sol. Energy Mater. Sol. Cells* **92**(11), 1305–1310 (2008).
22. D. Pierce and W. E. Spicer, "Electronic structure of amorphous Si from photoemission and optical studies," *Phys. Rev. B* **5**(8), 3017 (1972).

23. T. A. König et al., "Electrically tunable plasmonic behavior of nanocube–polymer nanomaterials induced by a redox-active electrochromic polymer," *ACS Nano* **8**(6), 6182–6192 (2014).
24. "Reference solar spectral irradiance: air mass 1.5," http://rredc.nrel.gov/solar/spectra/am1.5.
25. J. R. Nagel and M. A. Scarpulla, "Enhanced absorption in optically thin solar cells by scattering from embedded dielectric nanoparticles," *Opt. Express* **18**(S2), A139–A146 (2010).
26. J. Puhan et al., "An accurate representation of incoherent layers within one-dimensional thin-film multilayer structures with equivalent propagation matrices," *IEEE Photonics J.* **9**, 1–12 (2017).
27. A. Herman, M. Sarrazin, and O. Deparis, "The fundamental problem of treating light incoherence in photovoltaics and its practical consequences," *New J. Phys.* **16**(1), 013022 (2014).
28. G. S. Agarwal, G. Gbur, and E. Wolf, "Coherence properties of sunlight," *Opt. Lett.* **29**(5), 459–461 (2004).
29. A. Donges, "The coherence length of black-body radiation," *Eur. J. Phys.* **19**(3), 245 (1998).
30. M. Sarrazin, A. Herman, and O. Deparis, "First-principle calculation of solar cell efficiency under incoherent illumination," *Opt. Express* **21**(S4), A616–A630 (2013).

Maren Anna Brandsrud received her PhD in physics in 2020. She works currently as a postdoc in the BioSpec Group at the Faculty of Science and Technology at the Norwegian University of Life Sciences, in Ås, Norway. Her research interest is within light scattering and spectroscopy of small particles.

Reinhold Blümel is the Charlotte-Augusta-Ayres Professor of Physics at Wesleyan University, Connecticut, USA. He received his PhD from the Technical University in Munich in 1983 and his Habilitations degree in 1990. He is a fellow of the American Physical Society and recipient of the prestigious Heisenberg Fellowship. He has published more than 150 peer-reviewed papers in the scientific literature.

Rozalia Lukacs accepted her PhD in the field of theoretical physics in 2010 from Budapest University of Technology and Economics. She has been active in photonics research as a physicist for 12 years in several countries (Hungary, Norway, and USA). She studied the interaction of light and matter on atomic, micro- and nanoscale with computer simulations, theoretical modeling, and spectroscopy. She is currently working as a financial analyst at the Norwegian Public Service Pension Fund.

Eivind Seim received his PhD from the Norwegian University of Life Sciences in 2020. His research interests lie in the intersection of the fields of photovoltaics, chaos, and computational physics. After completing his PhD, he has been working for the Norwegian Public Service Pension Fund pursuing a career as a full stack developer.

Erik Stensrud Marstein is chief scientist at the Department for Solar Power Systems at the Institute for Energy Technology (IFE) in Norway, director of the Research Center for Sustainable Solar Cell Technology (FME SUSOLTECH), and adjoint professor in solar cell technology at the University of Oslo. He has been working at IFE in R&D in the field of PV since 2003. Most of his research has been performed in close collaboration with industry partners.

Espen Olsen: Biography is not available.

Achim Kohler received his PhD in physics in 1998. Currently, he is a professor in physics at the faculty of Science and Technology at the Norwegian University of Life Sciences, in Ås, Norway. He and his BioSpec Group are specialized in the field of vibrational spectroscopy of microorganisms and other micro-sized objects. He and his BioSpec Group have been keen on understanding and modeling of scattering and absorption in photonic micro- and nanosystems.